

1 Climatic Controls on Metabolic Constraints in the Ocean

2 Precious Mongwe^{1,2}, Matthew Long³, Takamitsu Ito⁴, Curtis Deutsch⁵, and Yeray
3 Santana-Falcón⁶

4 ¹Southern Ocean Carbon Climate Observatory (SOCCO), CSIR, Cape Town, South Africa

5 ²National Institute for Theoretical and Computational Sciences (NITheCS), [Cape Town](#), South Africa

6 ³Oceanography Section, Climate and Global Dynamics Laboratory, National Center for Atmospheric Research, Boulder, CO,
7 United States of America

8 ⁴School of Earth and Atmospheric Sciences, Georgia Institute of Technology, Atlanta, Georgia United States of America

9 ⁵Department of Geosciences, Princeton University, Princeton, NJ, United States of America

10 ⁶CNRM, Université de Toulouse, Météo-France, CNRS, Toulouse, 31057, France

11 **Corresponding Author:** Precious Mongwe (pmongwe@csir.co.za)

13 Abstract

14 Observations and models indicate that climate warming is associated with the loss of dissolved
15 oxygen from the ocean. Dissolved oxygen is a fundamental requirement for heterotrophic marine
16 organisms (except marine mammals) and, since the basal metabolism of ectotherms increases
17 with temperature, warming increases organisms' oxygen demand. Therefore, warming and
18 deoxygenation pose a compound threat to marine ecosystems. In this study, we leverage an
19 ecophysiological framework and compilation of empirical trait data quantifying the temperature
20 sensitivity and oxygen requirements of metabolic rates for a range of marine species
21 ("ecotypes"). Using the Community Earth System Model Large Ensemble, we investigate how
22 natural climate variability and anthropogenic forcing impact the ability of marine environments
23 to support aerobic metabolisms on interannual to multi-decadal timescales. Warming and
24 deoxygenation projected over the next several decades will yield a reduction in the volume of
25 viable ocean habitat. We find that fluctuations in temperature and oxygen associated with natural
26 variability are distinct from those associated with anthropogenic forcing in the upper ocean.
27 Further, the joint temperature-oxygen anthropogenic signal emerges sooner than [temperature and](#)
28 [oxygen](#) independently from natural variability. Our results demonstrate that anthropogenic
29 perturbations underway in the ocean will strongly exceed those associated with the natural
30 system; in many regions, organisms will be pushed closer to or beyond their physiological limits,
31 leaving the ecosystem more vulnerable to extreme temperature-oxygen events.

Formatted: Font: 9 pt

Formatted: Font: 9 pt

32 **1. Introduction**

33 Dissolved oxygen (O₂) is a fundamental metabolic requirement for heterotrophic marine
34 organisms, excluding marine mammals (Portner, 2002; Keeling et al., 2010; Tiano et al., 2014).

35 The decline ocean O₂ due to warming is a tendency long predicted by models (Keeling et al.,
36 2010; Long et al., 2016; Oschlies et al., 2018) and recently found evident at the global scale in
37 compilations of in situ observations (Schmidtko et al., 2017; Ito et al., 2017). Deoxygenation is
38 driven by the direct effect of reduced oxygen solubility with warming compounded by
39 buoyancy-induced stratification in the upper ocean, which weakens the ventilation-mediated
40 supply of fresh oxygen to the ocean interior. While the full ecological implications of ocean
41 deoxygenation remain uncertain, it is clear that the physiological impacts of oxygen loss on
42 marine organisms can be considered explicitly in the context of warming: basal metabolic rates
43 for ectothermic organisms depend on ambient temperature and increase with warming (Gillooly
44 et al., 2001); thus, higher temperatures impose additional demand for oxygen to sustain aerobic
45 respiration (Deutsch et al., 2015). Consequently, as the ocean warms, even present-day oxygen
46 distributions may be insufficient to meet the oxygen demands of organisms living near key
47 physiological thresholds (Deutsch et al., 2022).

48
49 Model projections clearly demonstrate that warming and deoxygenation are consequences of
50 human-driven climate change, yet natural climate variability also produces important
51 fluctuations in these quantities. Indeed, evidence suggests that natural variability contributes to
52 hypoxic events, such as those observed in the California Current, where fish and benthic-
53 organism mortality has been associated with low-O₂ waters impinging on the continental shelf
54 (Pozo Buil and Di Lorenzo, 2017; Howard et al., 2020). A clear understanding of how natural
55 climate variability drives fluctuations in metabolic state and the associated implications for
56 organisms is a critical context in which to view long-term climate warming. Given that the
57 natural system is highly dynamic, climate change signals are often masked by decadal-scale
58 variability (Ito and Deutsch, 2010). While numerous authors have considered detection and
59 attribution of climate change for physical and biogeochemical variables (Rodgers et al., 2015;
60 Long et al., 2016; Schlunegger et al., 2019), comparatively little attention has been devoted to
61 explicitly characterizing the relative influence of natural and anthropogenic drivers of changes in
62 the ocean's capacity to support aerobic life. In this study, we approach this challenge by

Deleted: is declining

Deleted: ,

Deleted: impacts

Deleted: While model

Deleted: it is important to recognize that

68 leveraging the concept of the Metabolic Index (Φ) introduced by Deutsch et al. (2015). Φ is
69 based on the notion that aerobic organisms can persist only where the ambient oxygen partial
70 pressure (pO_2) is sufficient to **sustain** respiration. Φ incorporates an explicit representation of the
71 dependence of metabolic oxygen demand on temperature, thus providing a framework to
72 consider how joint oxygen and temperature variability constrain viable habitat in the ocean.

Deleted: meet the requirements of sustaining

73
74 Many ocean organisms may already be under threat from deoxygenation (Hoegh-Guldberg and
75 Bruno, 2010; Breitburg et al., 2018); however, ongoing climate-driven loss of oxygen raises
76 important questions about the future of marine ecosystems: How will anthropogenic changes in
77 dissolved oxygen and temperature **affect** the capacity of ocean habitats to support aerobic
78 metabolism? What is the spatial and temporal distribution of changes in the ocean's metabolic
79 state associated with climate variability? At what point can anthropogenic change in the ocean's
80 metabolic state be distinguished from natural variability? This study addresses these questions
81 using a combination of metabolic theory, a dataset **quantifying key physiological parameters for**
82 a collection of marine species adapted to specific environments ("ecotypes"), and the oxygen and
83 temperature distributions **as** simulated in the Community Earth System Model, version 1 Large
84 Ensemble (CESM1-LE), which includes 34 members simulating ocean biogeochemistry under
85 climate variability and change from 1920–2100 forced using historical data and the
86 Representative Concentration Pathway Scenario 8.5 (RCP85) (Kay et al., 2015; Long et al.,
87 2016).

Deleted: impact

Deleted: set

88
89 This paper is organized as follows. Section 2 presents a brief overview of the relevant metabolic
90 theory, the associated empirical datasets, and describes our approach to analysis. In Section 3 we
91 present results quantifying the joint temperature-oxygen variability simulated in the CESM1-LE,
92 evaluating the spatiotemporal structure of variability in marine ecotype habitat, including long-
93 term trends based on the RCP8.5 scenario and time of emergence (ToE). The main outcomes of
94 the results are synthesized in Section 4 and summarized in Section 5.

96 **2. Datasets and methods**

97 **2.1 Metabolic index**

101 Empirical studies measuring thermal tolerance and oxygen requirements in the laboratory on an
 102 array of marine organisms have enabled an assessment of lethal thresholds (Vaquer-Sunyer and
 103 Duarte, 2008; Rosewarne et al., 2016). These data coupled with recent advances in a theoretical
 104 framework enable both explanatory and predictive power in the context of a dynamic
 105 environment (Deutsch et al., 2015; Penn et al., 2018; Howard et al., 2020). The fundamental
 106 insights here are that basal metabolic rates for ectothermic marine organisms depend on ambient
 107 temperature and generally increase with warming (Gillooly et al., 2001). Increasing basal
 108 metabolic rates impose additional demand for oxygen. Organisms use oxygen dissolved in
 109 seawater and acquisition tends to be limited by diffusive processes; thus, oxygen supply is
 110 related to the ambient pO_2 . The ratio of oxygen supply to temperature-dependent demand
 111 provides a critical indicator of the capacity for an organism to meet its metabolic requirements.
 112 Deutsch et al. (2015) formalized these concepts into a quantity termed the “Metabolic Index
 113 (Φ)”, which is defined as the ratio of oxygen supply to an organism’s resting metabolic demand.
 114 Oxygen supply is parameterized according to a biomass-dependent scaling of pO_2 , capturing
 115 variation in the efficiency with which organisms acquire and utilize O_2 . This can be expressed as
 116 $S = \alpha_s B^\sigma pO_2$, where α_s represent gas transfer between an organism and its environment and B^δ
 117 is the scaling of supply with biomass, B (Piiper et al., 1971). Gas supply is represented as an
 118 Arrhenius function;

$$119 \quad \alpha_s = \alpha_s \exp\left\{\frac{-E_s}{K_B} \left[\frac{1}{T} - \frac{1}{T_{ref}}\right]\right\} \quad (1)$$

120

121 Resting metabolic demand is also expressed using the Arrhenius equation as

$$122 \quad D = \alpha_D B^\delta \exp\left\{\frac{-E_d}{K_B} \left[\frac{1}{T} - \frac{1}{T_{ref}}\right]\right\}, \quad (2)$$

123 where α_D is a species-specific basal metabolic rate, E_d (eV) is the temperature dependence of
 124 oxygen supply, T is temperature, T_{ref} is the reference temperature (15°C), and k_B is the
 125 Boltzmann constant (Gillooly et al., 2001). Gas transfer is kinematically slow at low
 126 temperatures, and hence organism viability can be limited by the energy to acquire oxygen at low
 127 temperatures, thus E_o varies with temperature. Here we account for this by adding the
 128 temperature dependence (dE_o/dT) to E_o in equations above ($E_o + \frac{dE_o}{dT}(T - T_{ref})$), using the mean

129 value of $dE_o/dT = 0.022$ eV consistent with Deutsch et al. (2020). The Metabolic Index can thus
 130 be written as the ratio of S/D :

$$\begin{aligned}
 131 \quad \Phi &= \frac{\alpha_s B^\sigma}{\alpha_D B^\delta} pO_2 \exp\left\{\frac{-E_s}{K_B} \left[\frac{1}{T} - \frac{1}{T_{ref}}\right] + \frac{E_d}{K_B} \left[\frac{1}{T} - \frac{1}{T_{ref}}\right]\right\}, \\
 132 \quad &= A_o B^{\sigma-\delta} pO_2 \exp\left\{\frac{E_d - E_s}{K_B} \left[\frac{1}{T} - \frac{1}{T_{ref}}\right]\right\}, \\
 133 \quad &= A_o pO_2 \exp\left\{\frac{E_o}{K_B} \left[\frac{1}{T} - \frac{1}{T_{ref}}\right]\right\}, \tag{3}
 \end{aligned}$$

134 where $A_o = \alpha_s/\alpha_D$ (1/atm) is the hypoxic tolerance, $E_o = E_d - E_s$ (E_s is the temperature
 135 dependence of oxygen supply) (Deutsch et al., 2015; Penn et al., 2018). The exponent, $\varepsilon = \sigma -$
 136 δ , is the allometric scaling of the supply to demand ratio with biomass, is typically near zero.
 137 Therefore, in the analysis that follows, we presume unit biomass and thus neglect potential
 138 impacts of variations in biomass.

139
 140 If Φ falls below a critical threshold value of 1, conditions are physiologically unsustainable: an
 141 organism cannot meet its basic resting metabolic oxygen requirements. Conversely, values of Φ
 142 above 1 enable organismal metabolic rates to increase by a factor of Φ above resting levels,
 143 permitting critical activities such as feeding, defence, growth, and reproduction. Thus, for a
 144 given environment and species, Φ provides an estimate of the ratio of maximum sustainable
 145 metabolic rate to the minimum rate necessary for basal metabolism. Deutsch et al. (2015)
 146 inferred the ratio of active to resting energetic demand by examining the biogeographic
 147 distribution of several species, finding that range boundaries coincide with values of $\Phi = 1.5-7$.
 148 This threshold, termed critical rate (Φ_{crit}), represents the minimum metabolic index required for
 149 an organism to sustain an active metabolic state, which is a more meaningful ecological
 150 threshold than requirements for resting metabolism. Therefore, in this study, we define a quantity
 151 Φ' derived by dividing Φ by Φ_{crit} , so when Φ falls below 1, the organism can no longer sustain its
 152 active metabolic demand and will need to make physiological trade-offs. Accounting for these
 153 active metabolic requirements, we use an adjusted definition of the hypoxic tolerance trait, $A_c =$
 154 A_o / Φ_{crit} , where A_c is termed the “ecological hypoxia tolerance”, consistent with Howard et al.,
 155 2020. Where $\Phi' > 1$ (i.e., $\Phi > \Phi_{crit}$) an organism can sustain an active metabolic rate; where $\Phi' <$
 156 1 (i.e., $\Phi < \Phi_{crit}$), O_2 is insufficient and an active metabolic state is not viable. Henceforth, our

Deleted: Account

158 analysis focuses on Φ' ; in the subsequent metabolic index refers to Φ' ($\Phi' = \Phi$) throughout the
159 text and figures.

160

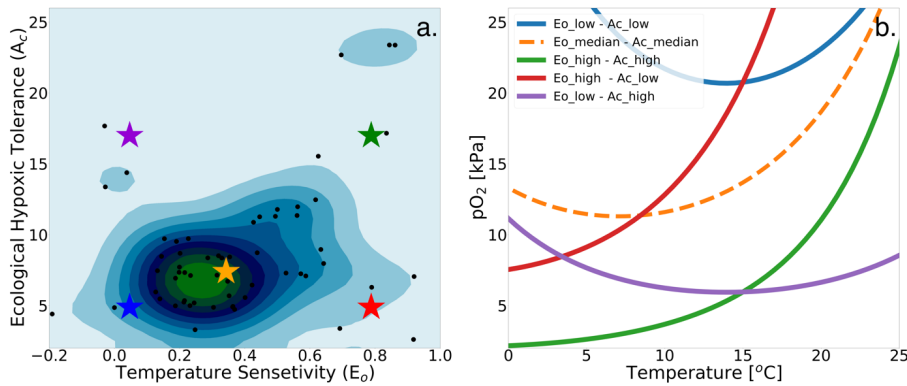
161 2.2 Physiological dataset

162 We make use of a dataset describing physiological parameters for a collection of 61 marine
163 ecotypes spanning a range of ecological hypoxic tolerances (A_c) and temperature sensitivities
164 (E_o) (Penn et al., 2018; Deutsch et al., 2020, Figure 1a). The 61 species span benthic and pelagic
165 habitats across four phyla in all ocean basins (Arthropoda, Chordata, Mollusca, and Cnidaria).
166 The dataset include 28 malacostracans, 21 fishes, three bivalves and cephalopods, two copepods,
167 and one each for gastropods, ascidians, scleractinian corals, and sharks with body mass spans of
168 eight orders of magnitude (Penn et al., 2018). We illustrate how the physiological traits E_o and A_c
169 constrain habitat viability in the context of distributions of pO_2 and temperature in the marine
170 environment in Figure 1b, which shows the minimum pO_2 (i.e., pO_2 at Φ_{crit}) required to sustain
171 an active metabolic state as a function of temperature for five combinations of E_o and A_c . The
172 five combinations are derived from sampling the probability distributions of E_o and A_c (Figure
173 1a) at the 10th, 50th, and 90th percentile values (illustrated by colored stars in Figure 1a and
174 corresponding curves in Figure 1b). We assume that the trait distributions are independent, which
175 is a reasonably modest simplification; E_o is represented by a normal distribution and A_c by a
176 lognormal distribution function (Figure S1). The pO_2 at Φ_{crit} curves shown in Figure 1b delineate
177 regions of pO_2 -temperature space that are habitable (above the curve) and uninhabitable (below
178 the curve). The reversing curvature of pO_2 at Φ_{crit} in Figure 1b at low temperature captures the
179 decrease of the organism's oxygen acquisition efficiency in cooler conditions yielding cold
180 intolerance. At very low temperatures, gas transfer is limited by the decrease in molecular gas
181 diffusion, as a consequence, oxygen transfer into the organisms requires energy, yielding cold

Deleted: =

Deleted: for

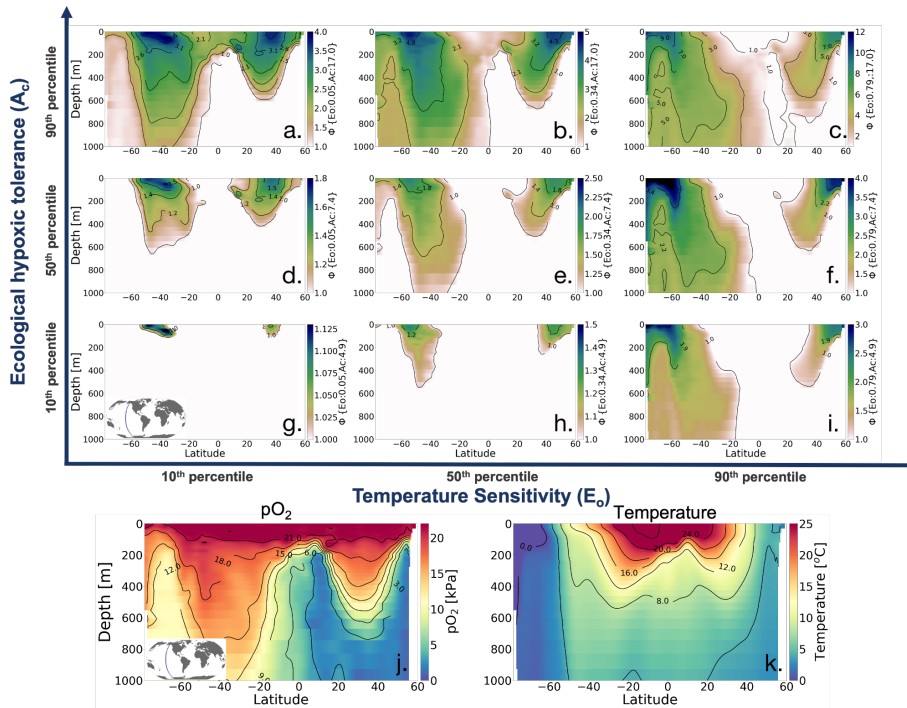
184 intolerance, this is well illustrating by the blue line in Figure 1b.



185
186 **Figure 1.** Physiological traits determining hypoxic tolerance. (a) Scatter plot of 61 marine ecotypes for which
187 empirically derived estimates of activation energy (E_o) and the ecological hypoxic tolerance (A_c) have been
188 determined (Penn et al., 2018). The color shows the density of occurrence for the 61 marine ecotypes in the $A_c - E_o$
189 trait space. (b) The minimum pO_2 required to sustain an active metabolic state (i.e., pO_2 at Φ_{crit} , Deutsch et al., 2020)
190 for five combinations of A_c and E_o corresponding to the stars in panel “a”; these are combinations of the 10th, 50th,
191 90th percentile values for each parameter. Below the pO_2 lines shown, the organism would experience an oxygen
192 deficit relative to its active metabolism requirements, effectively signifying the species-specific hypoxic conditions,
193 based on physiological traits, for this range of temperatures.

194
195 To illustrate how the trait combinations of E_o and A_c exert control on the geographic distribution
196 of organisms in the marine environment (Deutsch et al., 2020), we use observations of pO_2 and T
197 along a zonal transect of the Pacific Ocean and plot Φ' for nine combinations of E_o and A_c
198 percentile values (Figure 2). The colorbar in Figures 2a-i show the metabolic index for an active
199 state (Φ'); regions with values above one are habitable (color), while regions with values below
200 one are uninhabitable (white) on the basis of metabolic constraints (other ecological
201 considerations are not considered). The subplots in the upper portion of the figure are arranged
202 according to the same trait axes shown in Figure 1a; E_o increases horizontally from left to right
203 and A_c increases from the bottom to the top. For the trait combination in the bottom left (low E_o ,
204 low A_c ; Figure 2g), metabolism is relatively insensitive to temperature, and tolerance for low
205 pO_2 is poor. Thus, ecotypes with low E_o and low A_c are restricted to high latitude surface waters,
206 where temperatures are cool, and pO_2 is abundant (Figure 2g). As E_o increases from left to right,

207 metabolic rates become more sensitive to temperature. Then, habitat is gained at depth, where
 208 temperatures are cooler and higher temperature sensitivity confers an advantage (Figure 2g-i).
 209 From the bottom to the top, the increase in tolerance of low pO_2 conditions increases habitability
 210 in regions of low pO_2 , enabling organisms to expand beyond high-latitude surface waters (Figure
 211 2g-a). The biogeographic range for organisms with high A_c is modulated by E_o ; as temperature
 212 sensitivity increases, ecotype viability at high latitudes is increased, but tropical surface waters
 213 become less viable (Figure 2 a-c). Henceforth, our analysis will utilize the metabolic index of the
 214 median ecotype ($E_o = 0.34, A_c = 7.4$; Figure 2e) for illustrative purposes; i.e., all metabolic index
 215 figures refer to this median ecotype unless otherwise stated.



216
 217 **Figure 2.** Annual mean metabolic index (Φ) for nine combinations of the ecological traits E_o (metabolic
 218 temperature sensitivity) and A_c (ecological hypoxic tolerance) along a transect in the Pacific Ocean based on a
 219 climatology from the World Ocean Atlas dataset (Garcia et al., 2014). The percentile values of each trait are: 10th (E_o
 220 = 0.04, $A_c = 4.8$), 50th ($E_o = 0.34, A_c = 7.4$), and 90th ($E_o = 0.79, A_c = 17.0$). The lower panels show pO_2 and

221 temperature from the WOA dataset. Note that the colorbar range differs by panel and values where $\Phi' < 1$ are
222 omitted, thus the color shows only areas where an active metabolic state can be sustained.

223

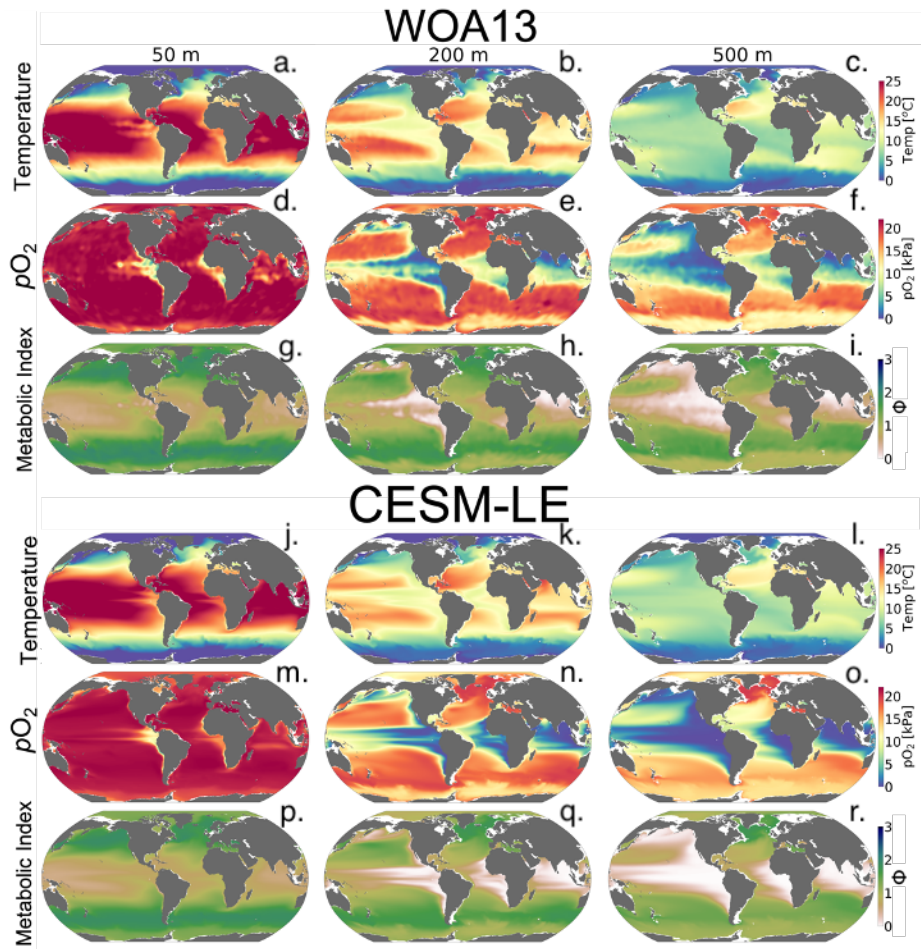
224 **2.3 Earth system model simulations**

225 This study is based on the CESM1-LE, described in detail by Kay et al. (2015). The CESM1-LE
226 included 34 ensemble members integrated from 1920–2100 under historical and RCP8.5 forcing.
227 The ensemble was generated by adding round-off level (10^{-14} K) perturbations to the air
228 temperature field at initialization in 1920; this small difference yields rapidly diverging model
229 solutions due to the chaotic dynamics intrinsic to the climate system, thus developing ensemble
230 spread representative of internal variability (Kay et al., 2015). Briefly, the CESM1-LE uses the
231 Community Earth System Model, version 1 (Hurrell et al., 2013), with a horizontal resolution of
232 nominally 1° in all components. The ocean component is Parallel Ocean Program version 2,
233 (Smith et al., 2010) with sea ice simulated by the Los Alamos Sea Ice Model version 4 (Hunke
234 and Lipscomb, 2010). Ocean biogeochemistry was represented by the Biogeochemical Elemental
235 Cycling (BEC) model (Moore et al., 2013; Lindsay et al., 2014).

236

237 Our analysis focuses on three depths: 50 m representing near-surface dynamics, the epipelagic
238 zone at 200 m, and the mesopelagic zone at 500 m. pO_2 was calculated using the Garcia and
239 Gordon. (1992) solubility formulation. For convenience, we use the period 1920–1965 to define
240 a minimally-perturbed natural state, as this period is prior to the development of substantial
241 anthropogenic trends in ocean oxygen and temperature (Long et al., 2016). We also examine
242 distributions over the last three decades of the 21st century (2070–2099) to evaluate the projected
243 climate-change signal under RCP8.5. We use the mean across all 34 ensemble members to
244 quantify the deterministic, “forced” response of the climate system to anthropogenic influence
245 (Deser et al., 2012). The ensemble spread is thus indicative of the amplitude of variations
246 attributable to natural variability.

247



248
 249 **Figure 3.** Mean-state comparison with observations. The climatological mean of (top rows) temperature (°C),
 250 (middle rows) pO_2 (kPa), and the (bottom rows) metabolic index for active metabolism (Φ') for the median ecotype
 251 ($E_o = 0.34$, $A_c = 7.4$); three depths are shown (left) 50 m, (center) 200 m, and (right) 500. Top panels show the
 252 WOA13 dataset and the bottom panels show CESM1-LE.

253
 254 We compared the CESM1-LE (1920 - 1965) with the World Ocean Atlas, version 2013
 255 (WOA2013) dataset (Garcia et al., 2014), an observationally-based, gridded climatology (Figure
 256 3a-i). CESM1-LE generally provides a reasonable representation of pO_2 and temperature

257 distributions at the selected depths (Figure 3); however, there are important biases to
258 acknowledge in the context of interpreting the results. Temperature magnitudes are generally
259 well simulated in the CESM1-LE, showing a root mean square error (RMSE) < 1.3 °C, and
260 pattern correlation coefficient (PCC) > 0.98 in all three selected depths (50 m, 200 m, and 500)
261 (Table 1). Temperature magnitudes are slightly underestimated at 50 m and 200 m (mean bias of
262 < 0.3 °C), and overestimated by 0.41 °C at 500 m. Note that since our comparison uses CESM1-
263 LE data from 1920-1965, some discrepancy in temperature might be expected from the signal of
264 climate warming present in the WOA observations. pO_2 is also reasonably well captured by the
265 CESM1-LE (PCC < 0.95), but magnitudes are slightly underestimated at depth, showing a mean
266 bias of -1.63 kPa and -2.1 kPa at 200 m and 500 m with respect to WOA13 (Table 1). Regions of
267 low pO_2 waters are too extensive in CESM1-LE (Figure 3n-o) and there is a slight degradation of
268 skill with depth for pO_2 fields (Table 1). The underestimation of pO_2 leads to a slight
269 underestimation of Φ' with respect to WOA13, and overestimate habitat loss in the future
270 climate (Figure 3 p-r); however, Φ' computed from the model fields demonstrates that the
271 dominant spatial patterns are well captured by the CESM1-LE despite magnitudes that are
272 slightly too low (i.e., Figure 1, c, l). This CESM pO_2 bias is common among coarse-resolutions
273 ocean models and it is attributed to a sluggish circulation and hence weak ventilation (Long et
274 al., 2016). These differences ultimately matter most near the hypoxic zones and at the boundaries
275 of habitable zones like the Oxygen Minimum Zones (OMZs).

276

277

278 **Table 1.** Summary statistics for the comparison of CESM1-LE with the World Ocean Atlas dataset (Garcia et al.,
 279 2014). The columns include the mean bias, pattern correlation coefficient (PCC), and root mean square error
 280 (RMSE) at 50 m, 200 m, and 500 m.

	Mean bias	R	RMSE
	Temperature [°C]		
50 m	-0.17	0.99	1.22
200 m	-0.25	0.99	1.22
500 m	0.10	0.98	0.63
	pO₂ [kPa]		
50 m	0.05	0.99	1.91
200 m	-1.17	0.96	5.96
500 m	-1.46	0.95	6.28
	Metabolic index		
50 m	0.01	0.99	0.02
200 m	-0.09	0.97	0.05
500 m	-0.15	0.96	0.08

Formatted Table

281
 282

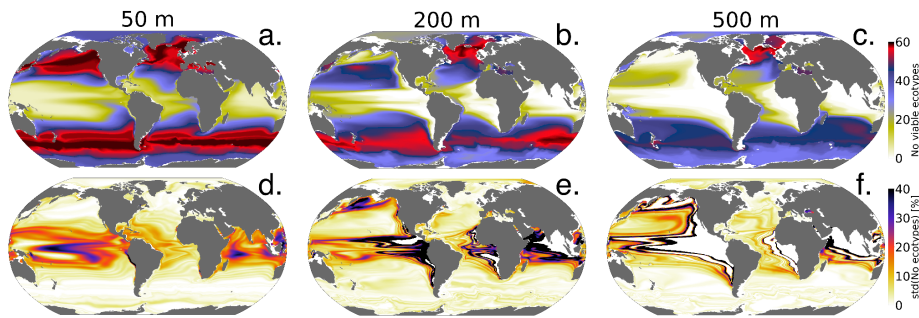
283 **2. Results**

284 **3.1 Joint temperature- pO_2 natural variability and forced trends**

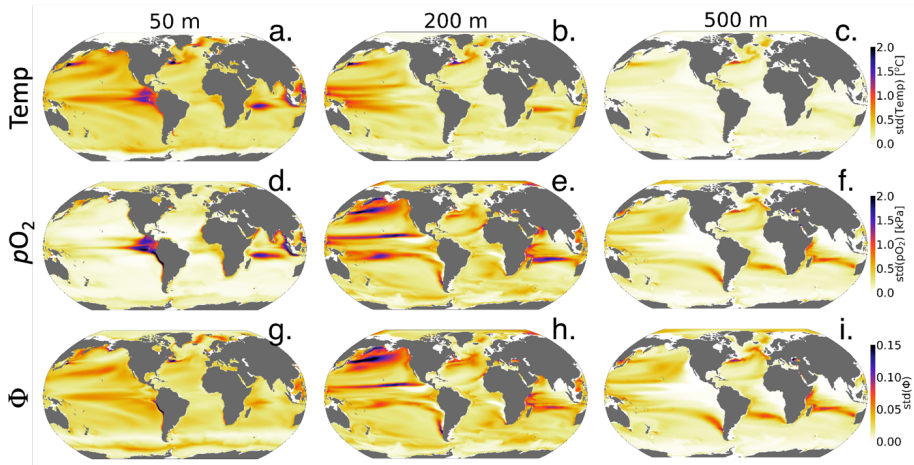
285
286
287 The spatial distribution of the number of viable ecotypes is shown in Figure 4 for the
288 “unperturbed” climate (1920-1965). Our intention here is not to quantify the actual
289 biogeographic range of organisms in the environment, but rather to illustrate the ocean’s ability
290 to support respiration by marine ectotherms given the metabolic capacities afforded within the
291 trait space of extant organisms. High latitude environments do not impose strong aerobic
292 constraints (cold intolerance notwithstanding), thus over much of the Southern Ocean, North
293 Atlantic, and Arctic Ocean almost all 61 ecotypes can sustain respiration. The tropical oceans
294 impose the strongest aerobic constraints, restricting the viability of ecotypes that do not have
295 high-hypoxia tolerance (A_o). For example, less than 25 ecotypes are viable over much of the
296 tropical surface ocean (Figure 4a); low concentrations of oxygen at depth impose even stronger
297 constraints, and no ecotypes are viable in the core of OMZs (Figure 4b, c). The spatial patterns of
298 the number of viable ecotypes is tightly controlled by temperature at the surface, since pO_2 is
299 mostly near saturated levels; at depth, however, pO_2 is the dominant driver of geographic
300 patterns in ecotype viability (Figures 2-4). Temperature generally decreases with depth, reducing
301 the metabolic oxygen demand. However, since pO_2 also decreases with depth and displays
302 greater lateral heterogeneity, pO_2 emerges as the dominant constraint of spatial structure in
303 ecotype viability at depth.

304
305 The standard deviation of annual anomalies using all CESM1-LE ensemble members provides
306 insight into the amplitude of natural variability (Figure. 5, one standard deviation). Temperature
307 and pO_2 show similar patterns of natural variability in the upper ocean, both showing particularly
308 large variance in the western tropical Pacific and Indian Ocean (Figure 5 a, d). Spatial variation
309 in the magnitude of temperature variability generally decreases with depth, but pO_2 displays even
310 relatively larger variability at depth with respect to the surface in some regions (Figure 5 a–f).
311 The joint pO_2 -temperature variability manifests in variations of Φ' (Figure 5g-i). Natural
312 variability in Φ' computed for the median ecotype shows spatial patterns similar to temperature

313 in the upper-surface ocean (50 m), but is more similar to pO_2 at depth. Thus, variations in Φ' tend
 314 to be temperature-dominated near the surface, but are more strongly controlled by pO_2 variability
 315 at depth. Φ' also shows the most extensive natural variability at 200 m consistent with the
 316 variability of pO_2 . The number of viable species shows more dramatic fluctuations than
 317 variations in the median ecotype Φ' ; variations in the number of viable ecotypes exceed 30% on
 318 annual timescales in the tropical upper ocean and near OMZ boundaries in the water column
 319 (Figure 4 c–d). This reflects the fact that interannual variability can preclude habitability for
 320 some regions of the A_c - E_o trait space, but these variations do not necessarily impact viability for
 321 the median ecotype (Figure 1). In the tropical surface ocean, high temperatures ($>25^\circ\text{C}$), and
 322 saturated surface ($pO_2 > 20$ kPa) require high hypoxia tolerance (A_c), but permit a range of
 323 E_o values (Figure 1b, 2a-b). Ecotypes with larger temperature sensitivity (high E_o) are
 324 particularly responsive to variations in temperature.
 325



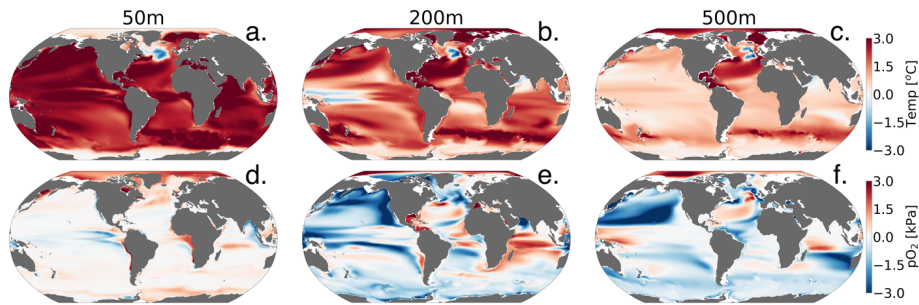
326
 327 **Figure 4.** Metabolic constraints on trait-space viability. Top row: the number of ecotypes from the physiological
 328 trait database that are viable (total = 61) in the CESM1-LE over the period 1920–1965. Bottom row: the standard
 329 deviation (expressed as a percent of the mean) in the number of viable ecotypes, reflecting fluctuations driven by
 330 natural variability.
 331



332
 333 **Figure 5.** The amplitude of natural variability in the ocean’s metabolic state. The panels show the standard deviation
 334 of annual-mean anomalies of all ensemble members over the period 1920–1965 for (top row) temperature (°C),
 335 (middle row) pO_2 (kPa), and (bottom row) the metabolic index (unitless) of the median ecotype ($E_o = 0.34$, $A_c = 7.4$).
 336

337 CESM1-LE simulates nearly homogeneous warming between 1920–1965 and 2070–2099 in the
 338 surface ocean (50 m) under RCP8.5, with an exception of the so-called North Atlantic warming
 339 hole (Figure 6a). Both modelling and observational studies have linked the North Atlantic
 340 warming hole to the slowing of the Atlantic overturning circulation with climate change (Keil et
 341 al., 2020). The magnitude of ocean warming generally diminishes with depth except in the North
 342 Atlantic, where, despite reductions, the overturning circulation effectively propagates
 343 anthropogenic heat anomalies into the ocean interior. pO_2 shows heterogeneous changes between
 344 1920–1965 and 2070–2099 (Figure 6 d-f). In the upper ocean, pO_2 changes are generally small (<
 345 1 kPa) because the near-surface is kept close to saturation via photosynthetic oxygen production
 346 and air-sea equilibration. At depth, however, pO_2 shows long-term changes linked to
 347 accumulated effects of respiration and changes in circulation (Ito et al., 2017). At 200 m for
 348 example, the Pacific Ocean displays a basin-wide mean reduction in pO_2 of 2 kPa (~30%), while
 349 the Atlantic and Indian basins gain about >2 kPa (~ 10 - 35%) by the end of the century. The
 350 largest long-term pO_2 loss (>3 kPa) occurs in the North Pacific while the largest pO_2 gain (~2

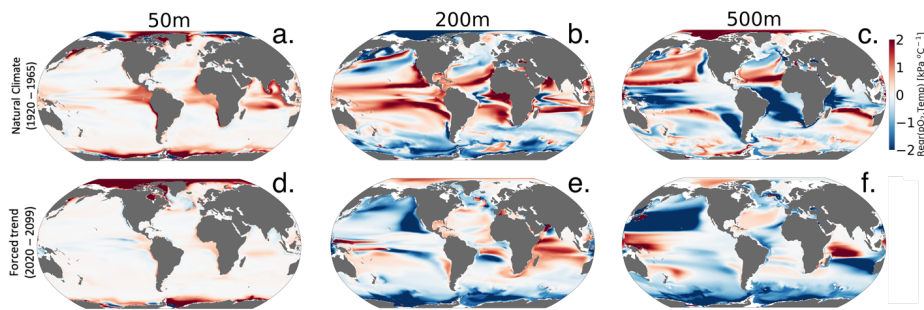
351 kPa) occurs in the North Atlantic gyre and western Indian Ocean (Figure 6 e-f).



352
353 **Figure 6.** Net long-term change (2070–2099 minus 1920–1965) in the CESM1-LE ensemble means temperature
354 (top) and (bottom) pO_2 at 50 m, 200 m, and 500 m.
355

356 Figure 7 shows the relationship between interannual variations in pO_2 versus temperature (pO_2 -
357 T) in the unperturbed climate (1920–1965; top row) and for the forced trend associated with 21st
358 century climate change (2070–2099 minus 1920–1965; bottom row). The nature of the pO_2 -T
359 relationship is an important indicator of the impacts of variability on the metabolic state.
360 Furthermore, the extent to which the forced trend is characterized by a pO_2 -T relationship that is
361 distinct from that associated with natural variability provides insight into the potential for
362 advanced or delayed detection of signals in Φ relative to pO_2 or temperature alone. Given that
363 metabolic rates for most organisms increase with temperature (positive E_o), a positive correlation
364 between variations in temperature and pO_2 is generally indicative of compensating changes,
365 wherein increased oxygen demand is at least partially offset by increased supply. Anticorrelation
366 between temperature and pO_2 , by contrast, will generally be associated with compounding
367 impacts on the metabolic index, as a negative correlation indicates that reductions in pO_2 (i.e.,
368 oxygen supply) accompany warming (i.e., increased demand). The sign of the pO_2 -T relationship
369 in the natural climate varies regionally and with depth (Figure 7, top row). The surface ocean is
370 generally characterized by a weak, positive pO_2 -T relationship, which could manifest from,
371 among other mechanisms, temperature-induced increases in photosynthetic oxygen production
372 (Figure 7a). The natural pO_2 -T relationship in the epipelagic (200 m) is characterized by strong
373 positive correlations in the tropics and negative correlations at high latitudes (Figure 7b). A
374 positive correlation between pO_2 and temperature at this depth could be induced by variability

375 associated with adiabatic vertical displacement of isopycnals, or “heave”, which has the effect of
 376 translating background gradients in properties vertically in the water column (Long et al., 2016).
 377 Upward movement of a deep isopycnal surface would yield a negative temperature anomaly and
 378 a negative pO_2 anomaly (positive correlation), as the deeper, colder waters have greater oxygen
 379 utilization signatures associated with longer ventilation age. Negative correlations between pO_2
 380 and temperature could manifest from ventilation processes, where enhanced subduction of
 381 surface water yields anomalously cold water masses that are enriched in oxygen. The sign of
 382 these epipelagic pO_2 -T correlations shows some similarity to those associated with the externally
 383 forced climate (Figure 6e), but the latter is characterized by a greater prevalence of
 384 anticorrelation, most notably in the North Pacific ocean. At 500 m depth, the relationship
 385 between temperature and pO_2 in the natural climate is almost a mirror image of the epipelagic
 386 (Figure 7c); the tropics generally display negative correlations, while polar regions show positive
 387 correlations (Figure 7 e). The pO_2 -T relationship in the forced trend at 500 m is dominated by
 388 broad regions of deeply negative correlations, with the most pronounced effect again in the
 389 North Pacific. The negative relationship is consistent with a ventilation signal, as buoyancy-
 390 induced stratification from warming curtails the introduction of new oxygen into the ocean
 391 interior. The predominantly negative pO_2 -T relationship associated with the forced trend is
 392 indicative of the compounding effects of climate change on metabolic state, increasing metabolic
 393 demand while simultaneously reducing oxygen supply.



394
 395 **Figure 7.** Regression of annual means pO_2 versus temperature ($kPa \text{ } ^\circ C^{-1}$) for (top row) interannual variability and
 396 (bottom row) the forced trend (difference between 2020–2099 and 1920–1965). The columns show the regressions
 397 computed at different depths, 50 m, 200 m, and 500 m, respectively.
 398

3.2 Long-term habitat changes

399
400

401 Figure 8 shows the climate-driven changes in Φ' for the median ecotype, as well as the impacts
402 of climate change on the number of viable ecotypes. Notably, while pO_2 in the near-surface
403 ocean is relatively insensitive to climate change (Figure 6d), there are reductions in Φ' in the
404 tropics (Figure 9d), owing to the direct impacts of warming. These changes are associated with
405 deep reductions in the number of viable ecotypes in the tropics (Figure 8a). There are modest
406 increases in Φ' and ecotype viability at high-latitudes; metabolic state in these regions is affected
407 by cold intolerance, thus warming broadens the viable region of trait space. Additionally, sea ice
408 melt support an increase in pO_2 , as gas exchange becomes more effective at restoring
409 equilibrium oxygen concentrations. The number of viable ecotypes shows more intense patterns
410 than those in the median ecotype Φ' in the upper ocean (Figure 8). This is partly because
411 ecotypes predicted to lose viability in the tropical regions ($\sim 50\%$) are at the extremes of the A_c -
412 E_o distribution (Figure 1) and not captured by the median ecotype Φ' . Nevertheless, outside the
413 tropical regions, the median ecotype gives a good indication of the anthropogenic impact to
414 marine ectotherms. The projected habitat loss in the epipelagic-pelagic North Pacific ($> 50\%$)
415 and habitat gain in the epipelagic-pelagic Southern Indian Ocean ($\sim 40\%$) and pelagic western
416 tropical regions ($\sim 40\%$) are consistent with a decrease in the median ecotype Φ' . Note that the
417 most pronounced effects on habitat are associated with regions where climate change drives a
418 strongly negative pO_2 -temperature relationship (Figure 7).

Deleted: reductions in

Deleted: cause

419
420

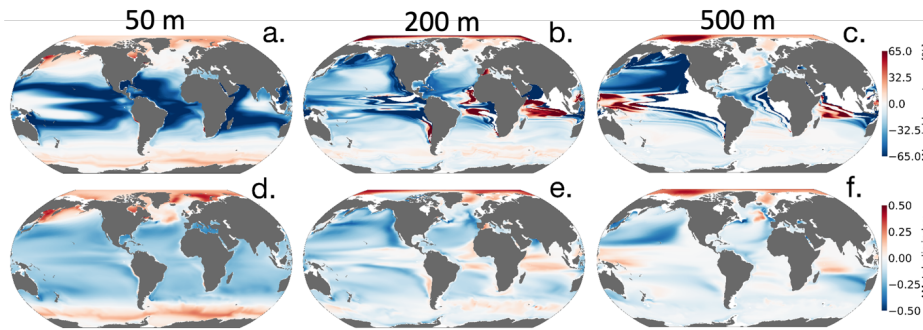


Figure 8. Net change in the number of habitable ecotypes in percentage (top row). Net metabolic index change

423 (2070 - 2099 vs. 1920 - 1965) for the median ecotype [$E_o = 0.34$, $A_e = 7.4$] (bottom row). At 50m (first column),
424 200m (second column) and 500m (third column).

425

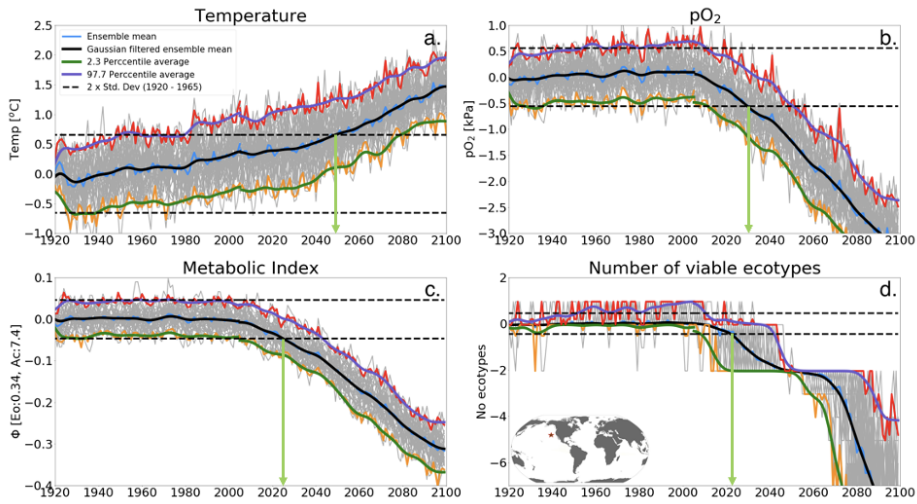
426 3.3 Time of Emergence

427

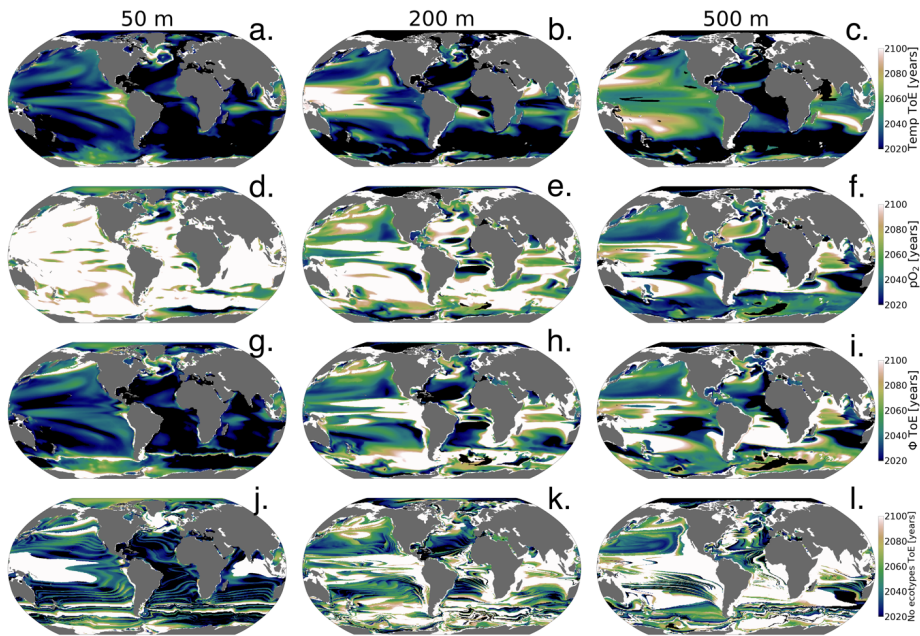
428 In this section, we examine the “time of emergence” (ToE, Hawkins and Sutton, 2012), the point
429 when forced changes in pO_2 , temperature and Φ' can be distinguished from the background
430 natural variability. We define ToE as the time when the magnitude of change in the ensemble
431 mean of a particular variable exceeds two standard deviations of the natural climate (1920 -
432 1965). This is illustrated in Figure 9 for a single grid point in the North Pacific at 200 m. At this
433 location, the forced trend in temperature shows a monotonic increase, while pO_2 shows a
434 monotonic decrease; as a result, Φ' for the median ecotype and the number of viable ecotypes
435 decrease over time. The anti-correlation between pO_2 and temperature exacerbates trends in Φ' ,
436 and hence the forced trend of the median ecotype Φ' emerges from natural noise earlier than
437 either pO_2 or temperature do alone (Figure 10a-c). Note that although the ToE of ecotype
438 viability change is directly derived from changes in Φ' , it is binary counted; changes in ecotype
439 viability are counted in whole numbers and this creates a step-function temporal-spatial variation
440 (Figure 9d). Consequently, this step-function-like feature of ecotype viability creates
441 discontinuities even in spatial patterns of ToE (Figure 10 j-l) as also shown in the natural
442 variance in Figure 4 d-f.

443

444



445
 446 **Figure 9.** Time of emergence (ToE) of the climate forcing signal for (a) temperature, (b) pO₂ (c) the metabolic
 447 index of the median ecotype [$E_o = 0.34$, $A_c = 7.4$], and (d) the number of viable ecotypes for a single model grid in
 448 the North Pacific at 200 m. ToE (green arrows) is defined as the time when the forced trend signal (ensemble
 449 member time series) is above two standard deviations (black dotted line) of all ensemble members for the period
 450 1920 - 1965.
 451

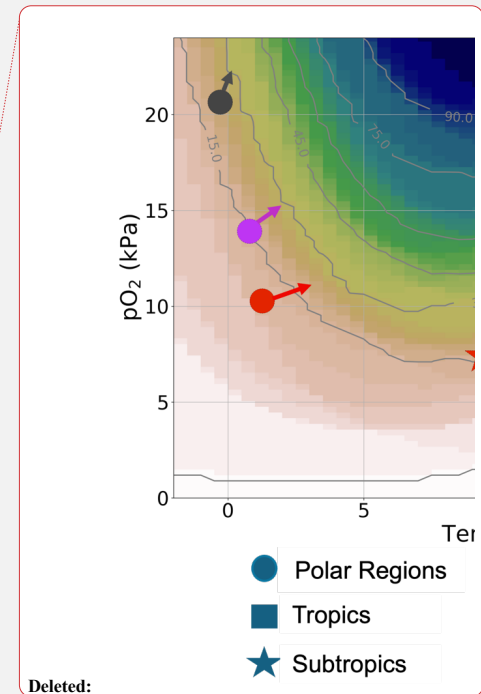


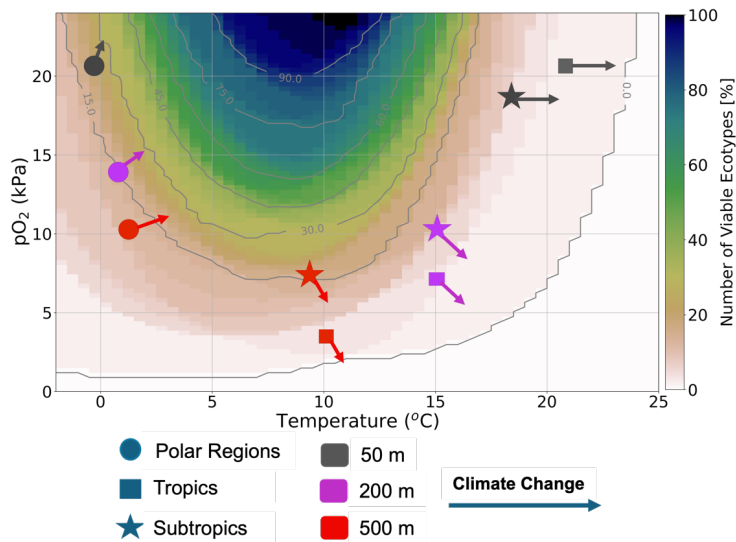
452
 453 **Figure 10.** Time of emergence (ToE) of the climate forcing signal for temperature, pO_2 , ϕ , and the number of
 454 viable ecotypes. ToE is defined as the time when the forced trend signal (ensemble member time series) is above
 455 two standard deviations of all ensemble members for the period 1920 - 1965.

456
 457 The ToE of pO_2 and temperature are inverted with depth; temperature emerges earliest in the
 458 upper ocean while pO_2 emerges earlier at depth and later or shows no emergence in the upper
 459 ocean (Figure 10 a-f). This feature is consistent with larger upper ocean temperatures long-term
 460 changes and greater pO_2 changes at depth. Near-surface ocean temperature has mostly already
 461 emerged by 2020 and is predicted to have almost completely emerged by the late 2060s under
 462 RCP85 (Figure 10 a-c). The early emergence of temperature from natural noise also persists for
 463 regions of relatively low natural variance at depth, e.g., the Southern Ocean and Atlantic Basin
 464 Gyres. Regions of the largest natural variability (see Figure 5) like the subtropical-subpolar
 465 Pacific however do not emerge until close to the end of the century. For pO_2 , anthropogenic
 466 changes in the upper ocean generally do not emerge from natural noise before the end of the
 467 century except for the Arctic Ocean and Eastern Antarctic. In the Arctic Ocean and Eastern

468 Antarctic pO_2 gain is related to sea-melt emergence by the mid-2050s (Figure 10a). The median
469 ecotype Φ' ToE shows spatial patterns that are coherent with temperature ToE in the upper ocean
470 with exception of polar regions. In contrast, they are consistent with pO_2 ToE patterns at depth;
471 this is consistent with net long-term Φ' changes in Figure 9d. The emergence of the
472 anthropogenic signal in ecotype viability closely resembles the median ecotype Φ' spatial
473 patterns but showing non-harmonious spatial patterns due to the step-function-like counting
474 feature of viability changes. It shows that the predicted $\sim 50\%$ ecotype viability loss in the
475 tropics (Figure 6a) may already be distinguishable from natural variability by the mid-2030s. In
476 the North Pacific, the predicted $> 50\%$ ecotype viability loss in the epipelagic-pelagic regions is
477 predicted to start emerging in the 2040s at 500 m and 2080s at 200 m (Figure 10 k-l).

478
479 In summary, we showed that because of the surface ocean's large warming signal and the least
480 pO_2 loss outside of the polar regions under the RCP85 climate scenario, it is characterized by
481 habitat loss in the tropics and a slight habitat gain in polar regions (Figure 11). Sea-ice melts
482 support Oxygen gain through the enhancement of temperature-driven solubility in the surface
483 polar regions. At depth, warming is less prevalent by the end of the 21st century; however,
484 oxygen loss related to the weakening ventilation of the ocean interior as the ocean becomes more
485 stratified has a stronger impact on metabolic reliance, leading to habitat loss in tropics and
486 subtropics. On the other hand, cooler temperatures and efficient ventilation in polar regions
487 create an oxygen-rich environment. Thus, in contrast to tropical and subtropical regions,
488 warming leads to a slight habitat gain (Figure 11), as organisms escape the cold intolerance
489 imposed by molecular gas diffusion at low temperatures.





491
 492 **Figure 11.** Summary Figure: It shows the distribution of ecotype viability within representative ocean temperature
 493 and pO_2 boundaries for the 66 species analysed in this study. The markers represent the subsampled regions, with
 494 polar regions denoted by circles, tropical regions by squares, and subtropical regions by stars. The colours represent
 495 the depth levels; 50 m (grey), 200 m (purple), and 500 m (red). Each arrow shows the estimated joint temperature-
 496 pO_2 climate change vector based on the net changes in temperature and pO_2 (as depicted in Figure 6).

497
 498 **4. Discussion**

499
 500 The human-induced rapid warming of the planet has been shown to drive ocean deoxygenation
 501 (Ito et al., 2017; Schmidtko et al., 2017; Long et al., 2016). Higher metabolic oxygen demand at
 502 higher temperatures (Gillooly et al., 2001; Deutsch et al., 2015, 2022) raises concerns about the
 503 ability of marine ectotherms to support aerobic respiration in the future. This study set out to
 504 characterize the anticipated climate change signal in the ocean's metabolic state in the context of
 505 natural variability using the metabolic theory as a basis to examine the capacity of the
 506 environment to support ectothermic marine heterotrophs.

507

508 The spatial variation in pO_2 and temperature in the unperturbed natural climate state set
509 biogeographic boundaries based on ectotherms' physiological performance. The resilience of
510 these ectotherms' biogeographic structure to natural variability and long-term climate warming is
511 perturbed by the joint pO_2 -temperature changes, effectively measured by the metabolic index
512 (Φ). An increase in the capacity of the organisms to support aerobic respiration increases Φ ; for
513 example by ocean cooling or increase in oxygen supply contrary, warming and decrease in
514 oxygen supply decrease Φ . There are exceptions in extremely low-temperature environments
515 (Figure 11), where aerobic respiration is also limited by kinematic gas transfer into the organism
516 in addition to environmental oxygen supply. Relative changes in pO_2 and temperature in the
517 natural variability and forced trend, therefore, regulate ectotherms' resilience to environmental
518 changes. Under the RCP85 climate scenario, the ocean generally warms homogeneously but
519 concurrent pO_2 changes are heterogeneous and vary with depth. Thus, the characteristics of these
520 pO_2 -temperature forced trend changes determine when the climate change impact on marine
521 ectotherms can be distinguishable from natural variability.

522
523 In the surface ocean, pO_2 is generally abundant and relatively uniform, and thus spatial
524 temperature variations have a dominant constraint on the spatial variations of organismic
525 metabolic state. The warmest parts of the surface ocean, the tropical oceans, can only support
526 about 10-20 (~ 30%) of the 61 ecotypes while cooler regions in the extra tropics have nearly
527 100% viability. Moreover, since warming anomalies propagate from the surface, the surface
528 tropical oceans also show the largest natural variance in temperature and ecotype viability. This
529 is because extremely warm temperatures in the surface tropics ($>25^\circ\text{C}$) are mainly suited for
530 organisms with high-temperature sensitivity (E_o), which are relatively fewer, and mostly close to
531 their physiological limits (Storch et al., 2014). Large natural variability in these warmest parts of
532 the tropical surface ocean precludes the forced trend signal from emerging from the natural
533 variability in the ecotype viability by end of the century although the ocean warms the largest in
534 the surface. Nevertheless, the large warming trends in the surface ocean generally emerge
535 relatively early (the 2020s) from natural variability in both temperature and ecotype viability in
536 most regions. Minimal changes in surface pO_2 in the forced trend affirm that surface ocean
537 marine ectotherms are mainly perturbed by temperature in the context of anthropogenic changes.
538 In polar regions, warming has a counterintuitive effect on marine ectotherms with respect to

Deleted: extratropics

540 most parts of the surface ocean. There, warming helps organisms escape extreme cold
541 intolerances by enhancing membrane kinematic gas transfer which enhances Φ' and thus ecotype
542 richness in the future (Figure 11)

543

544 In the epipelagic and mesopelagic regions (200 m and 500 m), the forced temperature trend and
545 natural variability are broadly smaller than the surface ocean, while pO_2 changes show the
546 opposite. Thus, at depth pO_2 play a more intricate role in perturbing marine ectotherm habitats
547 in the context of anthropogenic warming with respect to the surface ocean, where temperature
548 plays a dominant role. Contrasting the regression between pO_2 and temperature in the natural
549 climate, and forced trends provides an instructive framework to analysing ectotherms' long-term
550 changes. Regions showing different correlations between temperature and pO_2 in the forced
551 trends in comparison to the natural climate suggest a loss of metabolic resilience; loss of habitat,
552 and these regions tend to have a relatively early ToE. For instance, in the epipelagic and
553 mesopelagic North Pacific, temperature- pO_2 regressions switched from a positive correlation in
554 the unperturbed climate to a strong negative correlation in the forced trend (Figure 7). The North
555 Pacific pelagic – epipelagic regions is projected to lose nearly half of the present climate ecotype
556 viability by end of the 21st century, the projected habitat loss start emerging by the late 2030s
557 under the RCP85 climate scenario, On the other hand, in the Arctic Ocean and some parts of the
558 Southern Ocean, same sign pO_2 -temperature correlations in the forced trends result in the
559 preservation of the marine habitat and even slight enhancements.

560

561 **5. Conclusions**

562

563 The joint temperature-oxygen metabolic framework in this study provides additional insight into
564 the impact of climate change on marine ecosystems in comparison to the independent oxygen or
565 temperature analysis. We here showed that while warming is the leading order driving
566 mechanism of climate change, the direct effect of warming on marine ecosystems is mostly in
567 the upper ocean. Climate change-related oxygen loss is a major driver of marine ecosystem stress
568 in addition to warming at depth. Incorporating organismal physiological sensitivity to oxygen-
569 temperature changes in the metabolic framework provides insight into how climate impacts the

570 biogeographic structure of marine habitat. We find that forced perturbations to pO₂ and
571 temperature will strongly exceed those associated with the natural system in many parts of the
572 upper ocean, mostly pushing organisms in these environments closer to or beyond their
573 physiological limits. Climate warming is expected to drive significant marine habitat loss in the
574 surface tropical oceans and epipelagic - pelagic North Pacific Basin, while gaining marginal
575 habitat viability in the surface Arctic Ocean and some parts of the Ocean Southern.
576

577 **6. Competing interests**

578 The contact author has declared that none of the authors has any competing interests
579

580 **7. Acknowledgments**

581
582 PM, ML, CD and TI were funded by the National Science Foundation (NSF) grant agreement
583 No. 1737158. PM and YSF were also funded by the European Union's Horizon 2020 research
584 and innovation programme under grant agreement No. 820989 (COMFORT).). We also would
585 like to acknowledge the data access and computing support provided by the NCAR Cheyenne
586 HPC.

587 **8. Author contribution**

588
589 PM and ML designed the study approach. PM developed the analysis with feedback from ML,
590 CD and TI. PM prepared the manuscript with contributions from all co-authors.
591

592 **9. Data access**

593
594 The CESM1 large ensemble data used in this study can be accessed in this location:
595 <https://www.cesm.ucar.edu/community-projects/lens/data-sets>
596

597 **10. References**

598

599 Breitbart, D., Levin, L. A., Oschlies, A., Grégoire, M., Chavez, F. P., Conley, D. J., Garçon, V.,
600 Gilbert, D., Gutiérrez, D., Isensee, K., Jacinto, G. S., Limburg, K. E., Montes, I., Naqvi, S. W.
601 A., Pitcher, G. C., Rabalais, N. N., Roman, M. R., Rose, K. A., Seibel, B. A., Telszewski, M.,
602 Yasuhara, M., and Zhang, J.: Declining oxygen in the global ocean and coastal waters,
603 <https://doi.org/10.1126/science.aam7240>, 5 January 2018.

604
605 Deser, C., Phillips, A., Bourdette, V., and Teng, H.: Uncertainty in climate change projections:
606 The role of internal variability, *Clim Dyn*, 38, 527–546, [https://doi.org/10.1007/s00382-010-](https://doi.org/10.1007/s00382-010-0977-x)
607 [0977-x](https://doi.org/10.1007/s00382-010-0977-x), 2012.

608
609 Deutsch, C., Ferrel, A., Seibel, B., Pörtner, H. O., and Huey, R. B.: Climate change tightens a
610 metabolic constraint on marine habitats, *Science* (1979), 348, 1132–1135,
611 <https://doi.org/10.1126/science.aaa1605>, 2015.

612
613 Deutsch, C., Penn, J. L., and Seibel, B.: Metabolic trait diversity shapes marine biogeography,
614 *Nature*, 585, 557–562, <https://doi.org/10.1038/s41586-020-2721-y>, 2020.

615
616 Deutsch, C., Penn, J. L., Verberk, W. C. E. P., Inomura, K., Endress, M.-G., and Payne, J. L.:
617 Impact of warming on aquatic body sizes explained by metabolic scaling from microbes to
618 macrofauna, <https://doi.org/10.1073/pnas>, 2022.

619
620 Garcia, H. E. and Gordon, L. I.: Oxygen solubility in seawater: Better fitting equations,
621 <https://doi.org/10.4319/lo.1992.37.6.1307>, 1992.

622
623 Garcia, H. E. , Boyer, T. P. , Locarnini, R. A. , Antonov, J. I. , Mishonov, A. V. , Baranova, O.
624 K. , Melissa, M. Z. , Reagan, J. R. , and Johnson, D. R. .: *WORLD OCEAN ATLAS 2013*
625 *Volume 3: Dissolved Oxygen, Apparent Oxygen Utilization, and Oxygen Saturation*, 75,
626 <https://doi.org/10.7289/V5XG9P2W>, 2014.

627
628 Gillooly, J., Brown, J., West, G., Savage, V., Charnov, E., Gillooly, J. F., Brown, J. H., West, G.
629 B., Savage, V. M., and Charnov, E. L.: Effects of size and temperature on metabolic rate
630 Recommended Citation, 2001.

631
632 Hawkins, E. and Sutton, R.: Time of emergence of climate signals, *Geophys Res Lett*, 39,
633 <https://doi.org/10.1029/2011GL050087>, 2012.

634
635 Hoegh-Guldberg, O. and Bruno, J. F.: The Impact of Climate Change on the World's Marine
636 Ecosystems, *New Series*, 328, 1523–1528, <https://doi.org/10.1126/science.1185779>, 2010.

637 Howard, E. M., Penn, J. L., Frenzel, H., Seibel, B. A., Bianchi, D., Renault, L., Kessouri, F.,
638 Sutula, M. A., McWilliams, J. C., and Deutsch, C.: Climate-driven aerobic habitat loss in the
639 California Current System, 2020.

640

641 Hunke, E. C. and Lipscomb, W. H.: CICE: the Los Alamos Sea Ice Model Documentation and
642 Software User's Manual Version 4.1 LA-CC-06-012, 2010.

643

644 Hurrell, J. W., Holland, M. M., Gent, P. R., Ghan, S., Kay, J. E., Kushner, P. J., Lamarque, J. F.,
645 Large, W. G., Lawrence, D., Lindsay, K., Lipscomb, W. H., Long, M. C., Mahowald, N., Marsh,
646 D. R., Neale, R. B., Rasch, P., Vavrus, S., Vertenstein, M., Bader, D., Collins, W. D., Hack, J. J.,
647 Kiehl, J., and Marshall, S.: The community earth system model: A framework for collaborative
648 research, *Bull Am Meteorol Soc*, 94, 1339–1360, <https://doi.org/10.1175/BAMS-D-12-00121.1>,
649 2013.

650

651 Ito, T. and Deutsch, C.: A conceptual model for the temporal spectrum of oceanic oxygen
652 variability, *Geophys Res Lett*, 37, <https://doi.org/10.1029/2009GL041595>, 2010.

653

654 Ito, T., Minobe, S., Long, M. C., and Deutsch, C.: Upper ocean O₂ trends: 1958–2015, *Geophys*
655 *Res Lett*, 44, 4214–4223, <https://doi.org/10.1002/2017GL073613>, 2017.

656

657 Kay, J. E., Deser, C., Phillips, A., Mai, A., Hannay, C., Strand, G., Arblaster, J. M., Bates, S. C.,
658 Danabasoglu, G., Edwards, J., Holland, M., Kushner, P., Lamarque, J. F., Lawrence, D.,
659 Lindsay, K., Middleton, A., Munoz, E., Neale, R., Oleson, K., Polvani, L., and Vertenstein, M.:
660 The community earth system model (CESM) large ensemble project: A community resource for
661 studying climate change in the presence of internal climate variability, *Bull Am Meteorol Soc*,
662 96, 1333–1349, <https://doi.org/10.1175/BAMS-D-13-00255.1>, 2015.

663

664 Keeling, R. F., Körtzinger, A., and Gruber, N.: Ocean deoxygenation in a warming world, *Ann*
665 *Rev Mar Sci*, 2, 199–229, <https://doi.org/10.1146/annurev.marine.010908.163855>, 2010.

666 Keil, P., Mauritsen, T., Jungclaus, J., Hedemann, C., Olonscheck, D., and Ghosh, R.: Multiple
667 drivers of the North Atlantic warming hole, *Nat Clim Chang*, 10, 667–671,
668 <https://doi.org/10.1038/s41558-020-0819-8>, 2020.

669

670 Lindsay, K., Bonan, G. B., Doney, S. C., Hoffman, F. M., Lawrence, D. M., Long, M. C.,
671 Mahowald, N. M., Moore, J. K., Randerson, J. T., and Thornton, P. E.: Preindustrial-control and
672 twentieth-century carbon cycle experiments with the Earth system model CESM1(BGC), *J Clim*,
673 27, 8981–9005, <https://doi.org/10.1175/JCLI-D-12-00565.1>, 2014.

674

675 Long, M. C., Deutsch, C., and Ito, T.: Finding forced trends in oceanic oxygen, *Global*
676 *Biogeochem Cycles*, 30, 381–397, <https://doi.org/10.1002/2015GB005310>, 2016.

677
678 Moore, J. K., Lindsay, K., Doney, S. C., Long, M. C., and Misumi, K.: Marine ecosystem
679 dynamics and biogeochemical cycling in the community earth system model [CESM1(BGC)]:
680 Comparison of the 1990s with the 2090s under the RCP4.5 and RCP8.5 scenarios, *J Clim*, 26,
681 9291–9312, <https://doi.org/10.1175/JCLI-D-12-00566.1>, 2013.
682
683 Oeschlies, A., Brandt, P., Stramma, L., and Schmidtko, S.: Drivers and mechanisms of ocean
684 deoxygenation, <https://doi.org/10.1038/s41561-018-0152-2>, 1 July 2018.
685
686 Penn, J. L., Deutsch, C., Payne, J. L., and Sperling, E. A.: Temperature-dependent hypoxia
687 explains biogeography and severity of end-Permian marine mass extinction, *Science* (1979), 362,
688 <https://doi.org/10.1126/science.aat1327>, 2018.
689
690 Piiper, J., Dejours, P., Haab, P., and Rahn, H.: CONCEPTS AND BASIC QUANTITIES IN
691 GAS EXCHANGE PHYSIOLOGY, *Respiration Physiology*, 292–304 pp., 1971.
692 Portner, H. O.: Climate variations and the physiological basis of temperature dependent
693 biogeography: systemic to molecular hierarchy of thermal tolerance in animals, *Comparative*
694 *Biochemistry and Physiology Part A*, 739–761 pp., 2002.
695
696 Pozo Buil, M. and Di Lorenzo, E.: Decadal dynamics and predictability of oxygen and
697 subsurface tracers in the California Current System, *Geophys Res Lett*, 44, 4204–4213,
698 <https://doi.org/10.1002/2017GL072931>, 2017.
699
700 Rodgers, K. B., Lin, J., and Frölicher, T. L.: Emergence of multiple ocean ecosystem drivers in a
701 large ensemble suite with an Earth system model, *Biogeosciences*, 12, 3301–3320,
702 <https://doi.org/10.5194/bg-12-3301-2015>, 2015.
703
704 Rosewarne, P. J., Wilson, J. M., and Svendsen, J. C.: Measuring maximum and standard
705 metabolic rates using intermittent-flow respirometry: A student laboratory investigation of
706 aerobic metabolic scope and environmental hypoxia in aquatic breathers, *J Fish Biol*, 88, 265–
707 283, <https://doi.org/10.1111/jfb.12795>, 2016.
708
709 Schlunegger, S., Rodgers, K. B., Sarmiento, J. L., Frölicher, T. L., Dunne, J. P., Ishii, M., and
710 Slater, R.: Emergence of anthropogenic signals in the ocean carbon cycle, *Nat Clim Chang*, 9,
711 719–725, <https://doi.org/10.1038/s41558-019-0553-2>, 2019.
712
713 Schmidtko, S., Stramma, L., and Visbeck, M.: Decline in global oceanic oxygen content during
714 the past five decades, *Nature*, 542, 335–339, <https://doi.org/10.1038/nature21399>, 2017.
715 Smith, R., Jones, P., Briegleb, B., Bryan, F., Danabasoglu, G., Dennis, J., Dukowicz, J., Eden,
716 C., Fox-Kemper, B., Gent, P., Hecht, M., Jayne, S., Jochum, M., Large, W., Lindsay, K.,

717 Maltrud, M., Norton, N., Peacock, S., Vertenstein, M., and Yeager, S.: The Parallel Ocean
718 Program (POP) Reference Manual Ocean Component of the Community Climate System Model
719 (CCSM) and Community Earth System Model (CESM) 1, 2010.
720
721 Storch, D., Menzel, L., Frickenhaus, S., and Pörtner, H. O.: Climate sensitivity across marine
722 domains of life: Limits to evolutionary adaptation shape species interactions, *Glob Chang Biol*,
723 20, 3059–3067, <https://doi.org/10.1111/gcb.12645>, 2014.
724
725 Tiano, L., Garcia-Robledo, E., Dalsgaard, T., Devol, A. H., Ward, B. B., Ulloa, O., Canfield, D.
726 E., and Peter Revsbech, N.: Oxygen distribution and aerobic respiration in the north and south
727 eastern tropical Pacific oxygen minimum zones, *Deep Sea Res 1 Oceanogr Res Pap*, 94, 173–
728 183, <https://doi.org/10.1016/j.dsr.2014.10.001>, 2014.
729
730 Vaquer-Sunyer, R. and Duarte, C. M.: Thresholds of hypoxia for marine biodiversity, 2008.
731
732